Single-ion anisotropy is necessary and appropriate to study the magnetic behavior of Tb^{3+} moments with $J_{\rm eff} = \frac{1}{2}$ on the honeycomb lattice in $Tb_2Ir_3Ga_9$

Randy S. Fishman

Materials Science and Technology Division, Oak Ridge National Laboratory, Oak Ridge, 37831 Tennessee, USA

(Received 15 April 2021; revised 18 May 2021; accepted 1 June 2021; published 23 June 2021)

By developing models of increasing complexity, we show that a model without single-ion anisotropy (SIA) cannot explain the magnetic properties of $J_{\rm eff} = 1/2$ Tb^{3+} moments in the orthorhombically distorted, honeycomb material $Tb_2Ir_3Ga_9$. In four different models for the magnetization of a single honeycomb layer, the only sources of anisotropy are symmetric exchange interactions $J_{n\alpha\beta} = J_{n\beta\alpha}$ along three different bonds n, an anisotropic $\underline{g}$ tensor, and a Dzyalloshinskii-Moriya interaction (asymmetric exchange) that produces the observed canted moment along **b**. With 21 parameters, the best such model yields $\chi^2 = 0.065$, which is substantially smaller than $\chi^2 = 0.112$ obtained using a Heisenberg model containing six parameters including easy-axis anisotropy. However, models without SIA fail to reproduce the linear dependence of the magnetization with a field perpendicular to the Ising axis while predicting a saturation magnetization that is far too low. Due to the complex crystal-field environments, we argue that SIA is necessary to study low-symmetry, three-dimensional $J_{\rm eff} = 1/2$ materials containing Tb^{3+} ions.

DOI: 10.1103/PhysRevB.103.214440

I. INTRODUCTION

Driven by the search for spin liquids (SLs) and exotic quasiparticles like Majorana fermions, materials with effective spins of 1/2 have become a central focus in the study of quantum materials. For $J_{\rm eff} = 1/2$, $4d$ and $5d$ honeycomb materials like α-$RuCl_3$ [1–3] and A_2IrO_3 (A = Li, Na) [4–6], the Kitaev model [7–9] predicts that the different exchange couplings along the three nearest-neighbor bonds frustrate long-range magnetic order down to $T = 0$. As alternatives to $4d$ and $5d$ materials, rare-earth compounds like $YbMgGaO_4$, $YbCl_3$, and $TbInO_3$ have also been recently proposed as SL candidates [10–14]. One of the most popular building blocks for spin-ice and SLs is Tb^{3+}, which has quantum numbers $L = S = 3$ and $J = 6$, and a nominal g factor of 1.5. The 13 states in the $J = 6$ multiplet are split by crystal fields to yield a low-lying doublet with $J_{\rm eff} = 1/2$ and 11 higher levels. This ion forms the basis for several materials that do not magnetically order, such as the the SL candidate $TbInO_3$ [13], the quantum spin ice $Tb_2Ti_2O_7$ [15–17], and the spin glass $Y_{1-x}Tb_xNi_2Ge_2$ [18]. It also lays the foundation for many materials that do magnetically order, including three members of the RT_2X_2 (R = rare earth, T = transition metal, X = Si or Ge) family of intermetallic compounds: $TbNi_2Ge_2$ [19], $TbNi_2Si_2$ [20,21], and $TbCo_2Si_2$ [22–24]. Recently, $Tb_2Ir_3Ga_9$ (TIG) [25] joined this group of magnetically ordered materials.

Generally, crystal fields split the f-orbital J multiplet into a series of singlets, doublets, and triplets. If a low-lying doublet $|\Phi_\pm\rangle$ is sufficiently separated from higher-energy levels, then magnetic properties can be mapped onto an effective spin-1/2 model. For a Kramer's doublet with an odd number of f electrons, the off-diagonal matrix elements (with z taken along the Ising axis) $\langle\Phi_\pm|J_{iz}|\Phi_\mp\rangle$ vanish and the off-diagonal matrix elements $\langle\Phi_+|J_{i+}|\Phi_-\rangle$ and $\langle\Phi_-|J_{i-}|\Phi_+\rangle$ are nonzero. For a non-Kramer's doublet [17,26] with an even number of f electrons such as in the $4f^8$ shell of Tb^{3+}, $\langle\Phi_+|J_{i+}|\Phi_-\rangle$ and $\langle\Phi_-|J_{i-}|\Phi_+\rangle$ both vanish. Nevertheless, hybridization [26] with a nearby doublet $|\Xi_m\rangle$ due to spin interactions can generate nonzero off-diagonal matrix elements of $J_{i\pm} = J_{ix} \pm iJ_{iy}$. In either case, the spin-1/2 algebra is recovered by suitably rescaling the $\mathbf{J}_i$ operators and the exchange couplings. The angular momentum $\mathbf{J}_i$ can then be replaced by the $S = 1/2$ pseudospin operator $\mathbf{S}_i$. Ising-like behavior is produced when the $\underline{g}$ tensor has small components perpendicular to the Ising axis.

To describe $J_{\rm eff} = 1/2$ materials, models [10,11,27–29] for triangular and honeycomb lattices may contain diagonal terms $-J_{\alpha\alpha}S_{i\alpha}S_{j\alpha}$ coupling the same spin components and off-diagonal terms $-J_{\alpha\neq\beta}(S_{i\alpha}S_{j\beta} + S_{i\beta}S_{j\alpha})$ coupling different spin components on sites i and j. In addition to an anisotropic $\underline{g}$ tensor with different diagonal components $g_{\alpha\alpha}$ in a suitable local reference frame, some models also include asymmetric exchange or Dzyalloshinskii-Moriya (DM) terms like $D(S_{ix}S_{jy} - S_{iy}S_{jx})$. Noticeably absent from this list of possible interactions and anisotropies are terms that involve single-ion anisotropy (SIA). Since $\langle\Phi_\pm|S_{i\alpha}^2|\Phi_\pm\rangle$ is the same for each state in the low-lying doublet of $J_{\rm eff} = 1/2$ systems, SIA interaction terms like $-KS_{i\alpha}^2$ simply contribute a constant to the energy. Although it can be difficult to explain the properties of three-dimensional, magnetically ordered materials without invoking SIA associated with an easy axis or an easy plane, most model Hamiltonians used to describe $J_{\rm eff} = 1/2$ materials restrict consideration to the anisotropic exchange and $\underline{g}$-tensor terms described above.

II. TIG

Like many other Tb-based compounds, TIG contains $J_{\rm eff} = 1/2$ moments. This is unequivocally demonstrated by the λ

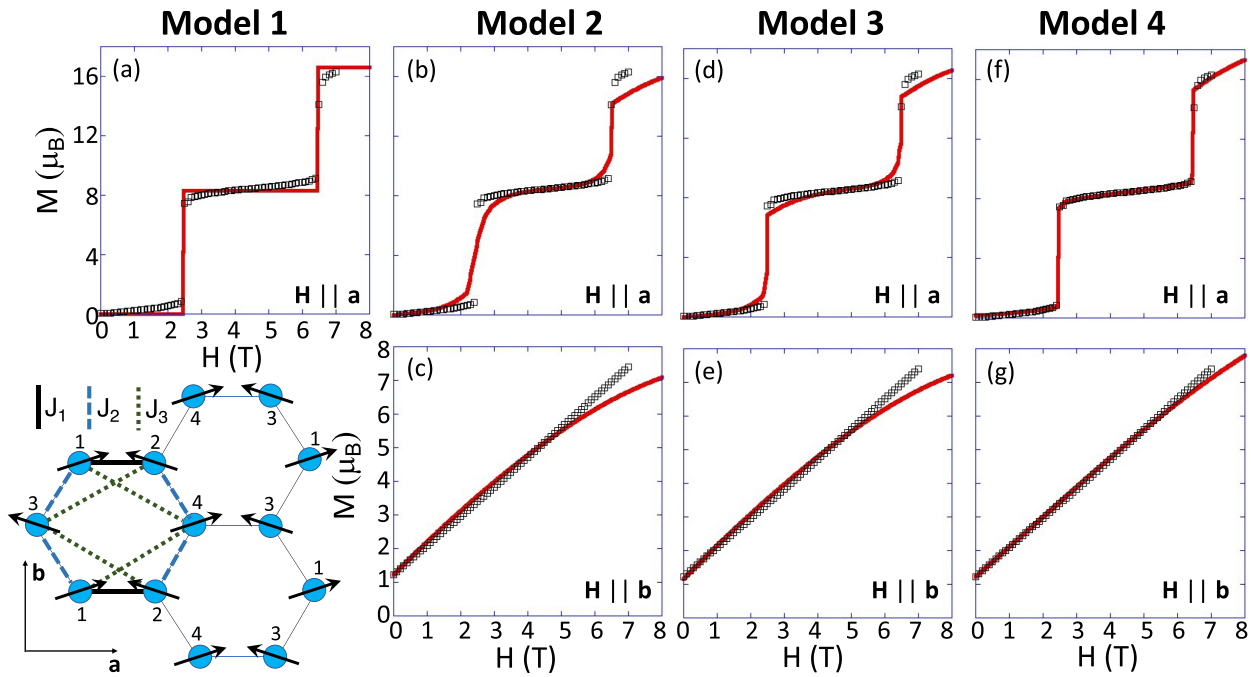

	Model 1	Model 2	Model 3	Model 4
J_{1xx}	-0.0297	-0.0298	-0.0344	-0.0192
J_{2xx}	-0.0149	-0.0172	-0.0162	-0.0290
J_{3xx}	-0.0067	-0.0076	-0.0073	-0.0047
J_{1yy}		-0.0031	-0.0047	-0.0012
J_{2yy}		-0.0025	-0.0021	-0.0075
J_{3yy}		-0.0006	-0.0006	-0.0023
J_{1xy}			-0.0036	0.0107
J_{2xy}			0.0020	-0.0037
J_{3xy}			0.0001	0.0044
J_{1zx}				0.0244
J_{1zy}				0.0480
J_{2zx}				0.0140
J_{2zy}				0.0076
J_{3zx}				0.0240
J_{3zy}				0.0024
J_{1zz}				0.0937
J_{2zz}				0.0511
J_{3zz}				0.0104
g_{xx}	1.382	1.426	1.464	1.614
g_{yy}		0.648	0.678	0.876
D		-0.0024	-0.0024	-0.0039
N	4	8	12	21
χ^2	0.755*	1.494	0.533	0.065

FIG. 1. Predictions (red curves) of four models compared with magnetization data (squares) for TIG. Below the graphs are the fitting parameters for each model. The symmetric exchange couplings $J_{n\alpha\beta}$ and DM interaction D are in meV with $S = 6$. N is the number of fitting parameters for each model. *For model 1, χ^2 only includes fits for field along **a**.

anomaly in its specific heat [25], which exhibits an $R\ln 2$ entropy characteristic of $J_{\rm eff} = 1/2$ moments. Also, like many other materials containing Tb^{3+} ions, TIG can be roughly described as Ising-like. At zero field, the four-sublattice spin configuration of each honeycomb layer is shown in the inset to Fig. 1. In a magnetic field along **a**, TIG exhibits two magnetization jumps seen in Fig. 1(a). These jumps are produced by the rotation of one spin in the ground state from $-\mathbf{a}$ to $+\mathbf{a}$ at $H_{c1} = 2.45$ T and of the other at $H_{c2} = 6.45$ T. Above 6.45 T, the magnetization approaches a fully saturated value close to

the free-ion value of $2\mu_B gS = 18\,\mu_B$ with $g = 3/2$ and $S = 6$ (all magnetization values are given per formula unit).

For angles η below about $\pi/3$, both $H_{c1}\cos\eta$ and $H_{c2}\cos\eta$ are roughly independent of η as the field **H** is rotated an angle η away from the a axis in the ab plane [25]. Hence, as befits an Ising-like material, the magnetic properties of TIG are predominantly determined by the component $H_x = H\cos\eta$ of the magnetic field along the a axis.

As shown in Fig. 1, the Tb^{3+} spins cant towards **b** in zero field. The zero-field canted moment of $M_0 = 1.22\,\mu_B$ obtained from magnetization measurements [25] can be explained by a DM interaction produced by the alternating positions of the Ir atoms around each hexagon. A somewhat larger canted moment of $2.06\,\mu_B$ was obtained using elastic neutron scattering [30]. Since models without SIA have difficulty reproducing this canted moment and the overall enhanced magnetization along **b**, we are providing the best-case scenario for those models by assuming the smaller value of $1.22\,\mu_B$.

In earlier work, Ye *et al.* [30] described both the magnetization and the inelastic neutron scattering spectra using a model Hamiltonian that contained two SIA terms: one to keep the spins in the ab plane and another to confine the spins to the a axis. This paper answers the obvious question: Can TIG be described by a model without SIA terms but rather with anisotropic exchange interactions and g tensor that are permitted for spin 1/2? To estimate the number N of parameters required to explain the magnetic behavior for a single honeycomb layer of TIG, we will build models of increasing complexity with N increasing from 4 to 21. Aside from model 1 (valid in one dimension only), all other models produce the same canted ground state.

III. TWO-DIMENSIONAL MODELS

A two-dimensional Kitaev-Heisenberg Hamiltonian for a single honeycomb layer is

$$\begin{aligned}\mathcal{H} = -\sum_{n,ij}\{&J_{nxx}S_{ix}S_{jx} + J_{nyy}S_{iy}S_{jy} + J_{nzz}S_{iz}S_{jz}\\ &+ J_{nxy}(S_{ix}S_{jy} + S_{iy}S_{jx}) + J_{nzx}(S_{iz}S_{jx} + S_{ix}S_{jz})\\ &+ J_{nzy}(S_{iz}S_{jy} + S_{iy}S_{jz})\} - K\sum_i S_{ix}^2\\ &+ \sum_{\langle ij\rangle}\mathbf{D}_{nij}\cdot(\mathbf{S}_i\times\mathbf{S}_j) - \mu_B\sum_{i,\alpha} g_{\alpha\alpha}H_\alpha S_{i\alpha}, \qquad (1)\end{aligned}$$

which includes all symmetric exchange interactions $J_{n\alpha\beta} = J_{n\beta\alpha}$ for each bond n with all spin and exchange indices in the laboratory reference frame of the crystal. Due to the small orthorhombic distortion of the lattice, bond 1 along the bottom and top of each hexagon parallel to **a** is treated differently from bond 2 along the sides of each hexagon. Bond 3 couples next-nearest neighbors on the diagonals of the hexagon.

While the SIA term $-KS_{iz}^2$ on each site generates an easy axis along **a**, the DM interactions $\mathbf{D}_{nij} = \pm D_n\mathbf{z}$ on bonds 1 and 2 couple all nearest neighbors $\{1,2\}$, $\{2,4\}$, $\{2,3\}$, $\{3,1\}$, and $\{3,4\}$ with alternating signs around each hexagon in Fig. 1. Because the fits described below did not improve with $D_1 \neq D_2$, we take $D_1 = D_2 = D$. The final term in Eq. (1) couples the spins $\mathbf{S}_i$ to a magnetic field **H** through the diagonal g-tensor components $g_{\alpha\alpha}$, again in the laboratory reference frame.

The energy $E = \langle\mathcal{H}\rangle$ is evaluated by taking each classical spin $\mathbf{S}_i$ to have a magnitude of $S = 6$. If the spins were instead defined to have a magnitude of $S = 1/2$, then the exchange and DM interactions would be multiplied by $6^2/(1/2)^2 = 144$ and the g-tensor components would be multiplied by $6/(1/2) = 12$. Due to the substantial interactions between honeycomb layers in TIG, quantum fluctuations are not expected to be significant and certainly cannot fix the deficiencies of models without SIA discussed below.

For simplicity, we confine consideration to a single honeycomb layer with fields along **a** and **b**. Due to the strong easy-plane anisotropy, the magnetization with field along **c** rises linearly [25] to about 1 μ_B at 7 T. As we shall see, the major shortcoming of models without SIA is that the g-tensor components g_{yy} and g_{zz} perpendicular to the Ising axis a must play two distinct roles: to provide an easy axis or easy plane ($g_{yy} \ll 1$ and $g_{zz} \ll 1$) and to determine the saturation magnetizations ($2g_{yy}\mu_B S$ and $2g_{zz}\mu_B S$) with fields along **b** and **c**. This will be amptly demonstrated by discussing the magnetization with the field along **b**. We only consider single honeycomb layers to avoid the unneccesary complexity of including additional exchange interactions between neighboring honeycomb layers, which are inequivalent [25] due to an offset along **b**.

With the field along **a**, χ^2 is evaluated using an experimental error of $\pm 6\%$ times the magnetization for fields above H_{c1}. Because the experimental results below H_{c1} are prone to uncertainties of unknown origin (such as crystal alignment, disorder, etc.), a constant magnetization error of $0.48\,\mu_B$ was used below H_{c1}. With the field along **b**, χ^2 uses an error of $\pm 6\%$ for all fields.

As verified by neutron scattering [30], the zero-field ground state in Fig. 1 is given by $\mathbf{S}_1 = \mathbf{S}_4 = S(\cos\psi, \sin\psi, 0)$ and $\mathbf{S}_2 = \mathbf{S}_3 = S(-\cos\psi, \sin\psi, 0)$, where $\psi = \sin^{-1}(M_0/2\mu_B g_{yy}S)$ is the canting angle of the spins with $M_0 = 1.22\,\mu_B$. For field along **b**, the magnetization rises linearly up to at least 7 T with $M(\mu_B) \approx 1.202 + 0.882\,H(\mathrm{T})$, as seen in Figs. 1 and 2.

To provide a baseline, we fit the magnetization data using a simple model that contains only three xy Heisenberg interactions $J_n \equiv J_{nxx} = J_{nyy}$, two g-tensor components g_{xx} and g_{yy}, and the SIA term K. Since the DM interaction is given by

$$D = \tfrac{1}{3}\{J_1 + 2J_2 - K\}\tan(2\psi), \qquad (2)$$

model H contains $N = 6$ parameters. As indicated above, ψ is the observed canting angle of the spins toward the **b** direction. With $\chi^2 = 0.112$, the predicted magnetizations together with the fitting parameters are given in Fig. 2. All Heisenberg interactions $J_n < 0$ are antiferromagnetic. For the field along **b**, model H predicts that $M(\mu_B) \approx 1.284 + 0.855\,H(\mathrm{T})$ between 0 and 7 T with a saturation magnetization of $2\mu_B g_{yy}S = 14.46\,\mu_B$.

We now compare the results of model H with the results of models without SIA, starting with a pure Ising model: $g_{yy} = 0$ and the only nonzero exchange interactions J_{nxx} act along the a axis. Since the spins are confined to the a axis, this model cannot explain the magnetization measurements along **b**. To

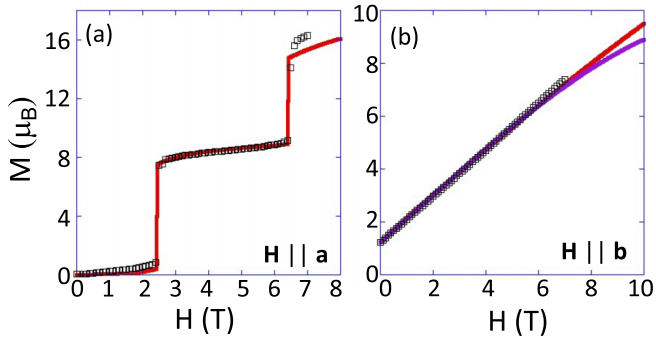

FIG. 2. Experimental data (squares) and predictions (red curves) of model H with $N = 6$ parameters, including easy-axis anisotropy $K = 0.0221$ meV. Other parameters are $J_1 = -0.0316$ meV, $J_2 = -0.0185$ meV, $J_3 = -0.0080$ meV, $g_{xx} = 1.458$, and $g_{yy} = 1.205$ with $\chi^2 = 0.112$. For comparison, the results of model 4 are plotted in the purple curve in (b).

obtain the observed ground state ($\mathbf{S}_1 = \mathbf{S}_4 = -\mathbf{S}_2 = -\mathbf{S}_3 = S\mathbf{a}$ without canting) and the measured critical fields $H_{c1} = 2.45$ T and $H_{c2} = 6.45$ T for the jumps in the magnetization, we require

$$g_{xx}\mu_B(H_{c1} + H_{c2}) = -2S(J_{1xx} + 2J_{2xx}), \tag{3}$$

$$g_{xx}\mu_B(H_{c2} - H_{c1}) = -8SJ_{3xx}, \tag{4}$$

along with the two inequalities $J_{1xx} < 4J_{3xx} < 0$ and $J_{2xx} < 2J_{3xx} < 0$.

Taking $g_{xx} = 1.382$, the saturation magnetization for field along **a** is $2\mu_B g_{xx} S = 16.58\ \mu_B$. While $J_{3xx} = -0.0067$ meV is fixed by the second equality above, the exchange interactions J_{1xx} and J_{2xx} lie within the ranges $-0.0327 < J_{1xx}(\text{meV}) < -0.0267$ and $-0.0164 < J_{2xx}(\text{meV}) < -0.0133$, subject to $J_{1xx} + 2J_{2xx} = -0.0594$ meV. Values in the middle of these ranges are given in column 1 of Fig. 1, with $J_{2xx} \approx J_{1xx}/2$. Corresponding to spins along $\pm\mathbf{a}$, each predicted magnetization plateau is completely flat. Containing only $N = 4$ parameters, model 1 yields $\chi^2 = 0.755$ for the magnetization along **a**. Not surprisingly, the J_{nxx} interactions are fairly close to the Heisenberg interactions of model H.

Note that all three bonds in Fig. 1 are required to predict the two observed jumps in the magnetization and that each bond has a unique value of J_{nxx}. Additional unique bonds would be required to describe $TbNi_2Ge_2$ [19] and $TbNi_2Si_2$ [20,21], which exhibit more than two magnetization jumps.

Model 2 builds on model 1 in two ways. First, we now include the DM interaction D, which is given in terms of the other fitting parameters J_{nxx} and J_{nyy} by

$$D = \tfrac{1}{6}\{3J_{1xx} + 6J_{2xx} - 4J_{3xx} + 2J_{1yy} + 4J_{2yy}\}\tan(2\psi). \tag{5}$$

With three exchange interactions J_{nyy} as well as g_{yy}, model 2 contains $N = 8$ parameters. Whereas the exchange interactions J_{nxx} in column 2 of Fig. 1 are quite similar to those obtained from model 1, the J_{nyy} parameters are an order of magnitude smaller. Although $g_{xx} = 1.426$ is also comparable to the result of model 1, $g_{yy} = 0.648$ is considerably smaller than g_{xx}. As seen in the second column of Fig. 1, the predicted magnetization with field along **a** exhibits a kink near H_{c1} and a small jump at H_{c2}. Because the spins are canted by the DM interaction at zero field, they can adjust to the presence of a field along **a** and the magnetization plateaus are no longer flat.

Since $D = -0.0024$ meV is given by Eq. (5), the predicted magnetization along **b** agrees with the measured value of 1.22 μ_B at zero field. Unlike the measured magnetization, however, the predicted magnetization grows linearly with field along **b** only up to about 4 T. This discrepancy proves to be the greatest shortcoming of models without SIA, which require that g_{yy} assumes two distinct roles. For the field along **b**, the largest observed magnetization at a field of 7 T is about 7 μ_B, much lower than the value of 16.3 μ_B with a 7 T field applied along **a**. A small value of $g_{yy} \ll g_{xx}$ is then required to constrain the predicted magnetization along **b**. But this small g_{yy} also predicts a low saturation magnetization of $2\mu_B g_{yy} S = 7.78\ \mu_B$, which is clearly inconsistent with the measurements. For model 2, the total χ^2 for the magnetizations along **a** and **b** is 1.494.

Model 3 adds the off-diagonal, symmetric exchange terms J_{nxy}. Because J_{nxy} produces different canting angles for spins 1 and 4 compared to spins 2 and 3, D becomes an additional fitting parameter so that $N = 12$. A major improvement in the fit to the magnetization along **a** can be seen in Fig. 1(d). While the predicted jump in the magnetization at H_{c2} is larger than for model 2, model 3 also predicts a distinct jump at H_{c1}. Notice that results for the directional exchange parameters J_{nxx} and J_{nyy} are quite similar to the results for models 1 and 2. With the addition of J_{nxy}, model 3 gives $\chi^2 = 0.533$.

Even with up to 12 parameters, these three models give substantially larger values of χ^2 than model H with only six parameters. Therefore, we now consider a final model without SIA that contains all symmetric exchange interactions $J_{n\alpha\beta} = J_{n\beta\alpha}$ for each bond. In addition to the parameters of model 3, model 4 includes the nine exchange couplings J_{nzx}, J_{nzy}, and J_{nzz}.

These new exchange interactions cause the spins to buckle out of the *ab* plane. Although no such buckling has been detected experimentally [25,30], the predicted buckling angle of $\tau_b = 0.053\pi$ for the spins is rather small and the buckling angle $g_{zz}\tau_b/g_{xx}$ for the magnetization will be even smaller. For the field along **a**, the azimuthal spin angles are $\theta_1 = \theta_4 = \pi/2 - \tau_b$ and $\theta_2 = \theta_3 = \pi/2 + \tau_b$ for $H < H_{c1}$ and $H > H_{c3}$. For $H_{c1} < H < H_{c2}$, $\theta_1 = \theta_3 = \pi/2 - \tau_b$ and $\theta_2 = \theta_4 = \pi/2 + \tau_b$. Notice that the predicted buckling of spin pairs $\{1, 2\}$ and $\{3, 4\}$ is antiferromagnetic. The zero-field buckling pattern does not change when a field is applied along **b**.

With D taken as one of $N = 21$ fitting parameters, model 4 gives $\chi^2 = 0.065$, which is about 42% lower than $\chi^2 = 0.112$ for model H. Results of model 4 for the magnetizations and fitting parameters are shown in column 4 of Fig. 1. While the fit to the data along **b** is still not satisfactory, model 4 does an excellent job at describing the data with the field along **a**. Surprisingly, $J_{1zz} = 0.094$ meV, $J_{2zz} = 0.051$ meV, and $J_{3zz} = 0.010$ meV are quite large and ferromagnetic. While $J_{1zx} = 0.024$ meV, $J_{1zy} = 0.048$ meV, $J_{2zx} = 0.014$ meV, and $J_{3zx} = 0.024$ meV are also large and ferromagnetic, the other off-diagonal components are rather modest. In model 4, the ferromagnetic parameters $J_{nz\alpha}$ involving the z component of the spin constrains the antiferromagnetic buckling of the spins

out of the plane. A model intermediate between models 3 and 4 (call it model 3.5) with no off-diagonal symmetric exchange on bond 3 gave a higher χ^2 of 0.287. So the new interactions on bond 3 are responsible for the additional improvements in model 4.

For the field along **b**, model 4 predicts that $M(\mu_B) \approx 1.288 + 0.854\,H(\mathrm{T})$ with a saturation magnetization of 10.51 μ_B. As shown in Fig. 2(b), the results of models 4 and H for the magnetization along **b** deviate above about 6 T.

IV. LIMITATIONS OF KITAEV MODEL

Despite the low χ^2 of model 4 and the rise of g_{yy} from models 2 through model 4, the predicted saturation magnetization of $2\mu_B g_{yy} S = 10.51\,\mu_B$ based on Kitaev physics is still far too low. When g_{yy} is no longer required to produce an easy axis, the saturation magnetization predicted by models with SIA [25,30] is consistently above 14 μ_B. The very large, ferromagnetic value of the exchanges $J_{n z\alpha}$ in model 4 is another signal that the absence of easy-plane anisotropy produces nonphysical results.

It is conceivable that a more complete model without SIA could improve upon model 4. Because it contains only one DM constant, model 4 does not include all three antisymmetric exchange interactions $\mathcal{J}_{n\alpha\beta} = -\mathcal{J}_{n\beta\alpha}$ on each bond n. Since there are a total of $3 \times 3 = 9$ exchange interactions on each bond, a complete model for a single honeycomb layer would contain $N = 9 \times 3\,(\mathrm{bonds}) + 2\,(g_{\alpha\alpha}) = 29$ parameters, eight more than model 4. But it is doubtful that even such a complete model will significantly increase the saturation magnetization with the field along **b**. Admittedly, it is also possible that we have not allowed sufficient time for the 21 parameters of model 4 to completely converge.

Thus far, we have only considered a single honeycomb layer. Modeling the stacked honeycomb layers of TIG in an *ABAB* pattern requires at least two more bonds between layers. So a full-fledged model of three-dimensional TIG without SIA would require $N = 9 \times 5\,(\mathrm{bonds}) + 3\,(g_{\alpha\alpha}) = 48$ parameters (34 if only symmetric exchange plus the DM interaction were included). Constructing such a model begs the question: At what point does a model contain so many parameters that it becomes effectively useless? While many of these parameters can likely be set to zero without increasing χ^2, it is necessary to start with the full gamut of parameters before they can be pared down. Recent work [30] used easy-plane and easy-axis anisotropies, five planar exchange couplings $J_{nxx} = J_{nyy}$, three exchange couplings J_{nzz}, and three g-tensor components ($N = 13$ parameters over five bonds [31]) to describe both the magnetization *and* inelastic spectra of TIG. It is hard to imagine a useful model that contains many more parameters.

Till now, Kitaev-Heisenberg models have been used to study materials with high symmetry, usually with only nearest-neighbor bonds. Since each of the three bonds on the triangular or honeycomb lattices are then related by symmetry, the total number of parameters is relatively small: up to seven parameters [10,28,32,33] for the rare-earth triangular-lattice $YbMgGaO_4$; up to six parameters including third-neighbor exchange [27,34] for the honeycombs Na_2IrO_3 and $\alpha-Li_2IrO_3$; up to five parameters [3,35] for the honeycomb $\alpha-RuCl_3$; and up to six parameters [17,26] for the spin-ice pyrochlore $Tb_2Ti_2O_7$. As far as we know, no model without SIA has been successfully applied to a material of such low symmetry as TIG.

Moreover, the role of spin-orbit coupling in TIG may not be completely addressed by the crystal-field splitting of the low-energy doublet. Recall that the non-Kramers Tb^{3+} doublet acquires nonzero off-diagonal matrix elements $\langle\Phi_\pm|J_{iy} \pm iJ_{iz}|\Phi_\mp\rangle$ when it hybridizes with a second doublet $|\Xi_m\rangle$ ($m = 1, 2$) lying Δ higher in energy. With a magnetic field along **b**, the zero-field doublet $|\Phi_\pm\rangle$ further changes to

$$|\Phi'_\pm\rangle = |\Phi_\pm\rangle - \sum_{m=1,2} |\Xi_m\rangle \frac{\mu_B g_{yy} H_y}{\Delta} \langle\Xi_m|J_{iy}|\Phi_\pm\rangle. \quad (6)$$

Using the value $\Delta = 1.7$ meV found for $Tb_2Ti_2O_7$ [17] and $g_{yy} = 0.84$, a 7 T field with $\mu_B g_{yy} H_y \sqrt{S}//\Delta \approx 0.6$ would significantly alter the hybridization between the two doublets and, consequently, the structure of the $J_{\mathrm{eff}} = 1/2$ doublet $|\Phi'_\pm\rangle$. A magnetic field along the Ising axis a does not significantly change the structure of the doublet $|\Phi'\pm\rangle$ because the ground-state doublet starts out with a diagonal matrix element for J_{ix} even before it hybridizes with $|\Xi_m\rangle$. So the easiest way to address the transitions between the two doublets due to a magnetic field along **b** may be through easy-axis anisotropy, which allows g_{yy} to produce the correct saturation magnetization.

Indeed, the symmetry of TIG may be so low that it does not even support a single low-lying doublet. As speculated in Ref. [25], the observed $R\ln 2$ entropy at the magnetic transition may be produced by two singlets that are close in energy, i.e., a pseudo doublet. Hence, applying the spin-1/2 algebra to TIG may be an oversimplification even in zero field. In addition, TIG does not meet the requirements [4] for edge-sharing octahedra that generate the off-diagonal exchange couplings in a $J_{\mathrm{eff}} = 1/2$ Kitaev model for oxides.

To add additional complexity, the stochiometry of TIG requires [36] that the Ir ions have a charge of -5 if the Ga ions have a charge of $+1$. This suggests that $5d$ electrons from Ir can hop onto the Tb sites to momentarily create $5d\ 4f^8$ Tb^{2+} ions, which have recently been studied in several molecule-based magnets [37–39]. The precise coupling mechanism (j-j or LS coupling) between the $5d$ electron and the $4f^8$ complex is the subject of some debate. It is possible that the transient formation of Tb^{2+} can produce a $J_{\mathrm{eff}} = 3/2$ state that is hospitable to SIA.

V. IS SIA MERELY NECESSARY OR ALSO APPROPRIATE?

After considering models of increasing complexity, we conclude that a model without SIA fails to predict the linear magnetization perpendicular to the Ising axis below 7 T for a single honeycomb layer of a $J_{\mathrm{eff}} = 1/2$ material. While it is remotely possible that a more complex model with all possible interactions can achieve this goal, it is highly unlikely that a tractable model without SIA can fully describe the three-dimensional properties of TIG. Since other magnetically ordered materials [19–21] containing Tb^{3+} ions exhibit even more complex behavior than TIG, SIA is necessary to study orthorhombically distorted $J_{\mathrm{eff}} = 1/2$ honeycomb systems when a field is applied perpendicular to the Ising axis.

Nevertheless, model 4 without SIA had no difficulty describing the magnetization measurements of TIG when a field was applied parallel to the Ising axis. Restricted to a field applied along the Ising axis or to zero field, a model without SIA may then be appropriate to study the properties of a distorted, three-dimensional compound containing Tb^{3+} ions. Because such a model would require more than 34 parameters, however, it would not be realistic.

This discussion implies that a model containing SIA is necessary to study three-dimensional, $J_{\rm eff} = 1/2$ materials of low symmetry. But it does not answer the deeper question whether such a model is also appropriate. For the reasons given above, a $J_{\rm eff} = 1/2$ model oversimplifies the complex physics of low-symmetry materials like TIG. To describe these materials, a $J_{\rm eff} = 1/2$ model without SIA has no better justification than a $J = L + S > 1/2$ model with SIA. Both types of models oversimplify the splitting of a J multiplet in a very low-symmetry environment. With a magnetic field applied perpendicular to the Ising axis, treating an orbitally coupled multiplet as $(2J + 1)$-degenerate is just as erroneous as treating it as twofold degenerate.

From a phenomenological point of view, the advantage of taking the spin S to be greater than $1/2$ is that it can then be treated as another fitting parameter. To evaluate the magnetization and critical fields, the scaled exchange $\tilde{J}_{ij} = S^2 J_{ij}$, the SIA $\tilde{K} = S^2 K$, the DM interaction $\tilde{D} = S^2 D$, and the $\underline{g}$-tensor $\tilde{g}_{\alpha\beta} = S g_{\alpha\beta}$ enter the classical energy $\tilde{E} = S^2 E$ on equal levels. While the magnetization M_x is proportional to $\tilde{g}_{xx}{\mu_{\rm B}}^2 H_x/\tilde{J}_{xx}$, the critical fields H_{c1} and H_{c2} in Eqs. (3) and (4) are proportional to $\tilde{J}_{xx}/\mu_{\rm B}\tilde{g}_{xx}$, all independent of S. To leading order in $1/S$, the Néel temperature is also independent of S and proportional to $(z/3)|\tilde{J}_{ij}|$, where z is the number of nearest neighbors. In a spin-wave expansion about the classical limit, the spin-wave frequencies $\hbar\omega_{\rm sw}$ are proportional to $\tilde{J}_{ij}/S$ with an overall energy scale set by $1/S$ (the next-order corrections are of order $\tilde{J}_{ij}/S^2$). Hence, the effective value for the spin S can be determined by simultaneously fitting the magnetization and spin-wave data. We shall employ this technique in future work.

While the relative justifications of models with and without SIA can be endlessly debated, the utility and simplicity of models containing SIA cannot be denied. Whereas applications of $J_{\rm eff} = 1/2$ models to systems of low symmetry provide results that are difficult to interpret physically, models with SIA provide results that are easy to understand and have direct physical consequences. We argue that a Heisenberg model containing SIA with an effective spin greater than $1/2$ provides a much easier path to model and understand distorted honeycomb systems with nominal doublet ground states.

ACKNOWLEDGMENTS

The authors would like to acknowledge useful conversations with A. Chernyshev, J. Gardner, M. Khan, J. Mitchell, M. Whangbo, F. Ye, and V. Zapf. Research was sponsored by the U.S. Department of Energy, Office of Basic Energy Sciences, Materials Sciences and Engineering Division.

[1] L. Ding, J. Koo, L. Xu, X. Li, X. Lu, L. Zhao, Q. Wang, Q. Yin, H. Lei, B. Yan, Z. Zhu, and K. Behnia, Intrinsic Anomalous Nernst Effect Amplified by Disorder in a Half-Metallic Semimetal, Phys. Rev. X **9**, 041061 (2019).

[2] K. W. Plumb, J. P. Clancy, L. J. Sandilands, V. V. Shankar, Y. F. Hu, K. S. Burch, H.-Y. Kee, and Y.-J. Kim, α-$RuCl_3$: A spin-orbit assisted Mott insulator on a honeycomb lattice, Phys. Rev. B **90**, 041112(R) (2014).

[3] A. Banerjee, C. A. Bridges, J.-Q. Yan, A. A. Aczel, L. Li, M. B. Stone, G. E. Granroth, M. D. Lumsden, Y. Yiu, J. Knolle, S. Bhattacharjee, D. L. Kovrizhin, R. Moessner, D. A. Tennant, D. G. Mandrus, and S. E. Nagler, Proximate Kitaev quantum spin liquid behaviour in a honeycomb magnet, Nat. Mater. **15**, 733 (2016).

[4] G. Jackeli and G. Khaliullin, Mott Insulators in the Strong Spin-Orbit Coupling Limit: From Heisenberg to a Quantum Compass and Kitaev Models, Phys. Rev. Lett. **102**, 017205 (2009).

[5] J. Chaloupka, G. Jackeli, and G. Khaliullin, Kitaev-Heisenberg Model on a Honeycomb Lattice: Possible Exotic Phases in Iridium Oxides A_2IrO_3, Phys. Rev. Lett. **105**, 027204 (2010).

[6] Y. Singh, S. Manni, J. Reuther, T. Berlijn, R. Thomale, W. Ku, S. Trebst, and P. Gegenwart, Relevance of the Heisenberg-Kitaev Model for the Honeycomb Lattice Iridates A_2IrO_3, Phys. Rev. Lett. **108**, 127203 (2012).

[7] A. Kitaev, Anyons in an exactly solved model and beyond, Ann. Phys. **321**, 2 (2006).

[8] W. Witczak-Krempa, G. Chen, Y. B. Kim, and L. Balents, Correlated quantum phenomena in the strong spin-orbit regime, Annu. Rev. Condens. Matter Phys. **5**, 57 (2014).

[9] H. Takagi, T. Takayama, G. Jackeli, G. Khaliullin, and S. E. Nagler, Concept and realization of Kitaev quantum spin liquids, Nat. Rev. Phys. **1**, 264 (2019).

[10] Y. Li, H. Liao, Z. Zhang, S. Li, F. Jin, L. Ling, L. Zhang, Y. Zou, L. Pi, Z. Yang, J. Wang, Z. Wu, and Q. Zhang, Gapless quantum spin liquid ground state in the two-dimensional spin-1/2 triangular antiferromagnet $YbMgGaO_4$, Sci. Rep. **5**, 16419 (2015).

[11] Y. Li, G. Chen, W. Tong, L. Pi, J. Liu, Z. Yang, X. Wang, and Q. Zhang, Rare-Earth Triangular Lattice Spin Liquid: A Single-Crystal Study of $YbMgGaO_4$, Phys. Rev. Lett. **115**, 167203 (2015).

[12] J. Xing, E. Feng, Y. Liu, E. Emmanouilidou, C. Hu, J. Liu, D. Graf, A. P. Ramirez, G. Chen, H. Cao, and N. Ni, Neel-type antiferromagnetic order and magnetic field–temperature phase diagram in the spin-1/2 rare-earth honeycomb compound $YbCl_3$, Phys. Rev. B **102**, 014427 (2020).

[13] L. Clark, G. Sala, D. D. Maharaj, M. B. Stone, K. S. Knight, M. T. F. Telling, X. Wang, X. Xu, J. Kim, Y. Li, S.-W. Cheong, and B. D. Gaulin, Two-dimensional spin liquid behaviour in the triangular-honeycomb antiferromagnet $TbInO_3$, Nat. Phys. **15**, 262 (2019).

[14] J. Kim, K. M. Rabe, and D. Vanderbilt, Negative piezoelectric response of van der Waals layered bismuth tellurohalides, Phys. Rev. B **100**, 104115 (2019).

[15] J. S. Gardner, S. R. Dunsiger, B. D. Gaulin, M. J. P. Gingras, J. E. Greedan, R. F. Kiefl, M. D. Lumsden, W. A. MacFarlane, N. P. Raju, J. E. Sonier, I. Swainson, and Z. Tun, Cooperative Paramagnetism in the Geometrically Frustrated

Pyrochlore Antiferromagnet $Tb_2Ti_2O_7$, Phys. Rev. Lett. **82**, 1012 (1999).

[16] M. J. P. Gingras, B. C. D. Hertog, M. Faucher, J. S. Gardner, S. R. Dunsiger, L. J. Chang, B. D. Gaulin, N. P. Raju, and J. E. Greedan, Thermodynamic and single-ion properties of Tb^{3+} within the collective paramagnetic-spin liquid state of the frustrated pyrochlore antiferromagnet $Tb_2Ti_2O_7$, Phys. Rev. B **62**, 6496 (2000).

[17] H. R. Molavian, M. J. P. Gingras, and B. Canals, Dynamically Induced Frustration as a Route to a Quantum Spin Ice State in $Tb_2Ti_2O_7$ Via Virtual Crystal Field Excitations and Quantum Many-Body Effects, Phys. Rev. Lett. **98**, 157204 (2007).

[18] T. A. Wiener, I. R. Fisher, S. L. Bud'ko, A. Kracher, and P. C. Canfield, Design of a metallic ising spin glass in the $Y_{1-x}Tb_xNi_2Ge_2$ system, Phys. Rev. B **62**, 15056 (2000).

[19] S. L. Bud'ko, Z. Islam, T. A. Wiener, I. R. Fisher, A. H. Lacerda, and P. C. Canfield, Anisotropy and metamagnetism in the RNi_2Ge_2 (R=Y, La-Nd, Sm-Lu) series, J. Magn. Magn. Mater. **205**, 53 (1999).

[20] J. A. Blanco, D. Gignoux, D. Schmitt, and C. Vettier, Field induced magnetic structures in $TbNi_2Si_2$, J. Magn. Magn. Mater. **97**, 4 (1991).

[21] T. Shigeoka, H. Fujii, M. Nishi, Y. Uwatoko, T. Takabatake, I. Oguro, K. Motoya, N. Iwata, and Y. Ito, Metamagnetism in $TbNi_2Si_2$ single crystal, J. Phys. Soc. Jpn. **61**, 4559 (1992).

[22] N. Iwata, K. Honda, T. Shigeoka, Y. Hashimoto, and H. Fujii, Metamagnetism in $DyCo_2Si_2$, J. Magn. Magn. Mater. **90-91**, 63 (1990).

[23] L. Vinokurova, V. Ivanov, and A. Szytula, Magnetic phase diagrams of $TbCo_2Si_2$, $DyCo_2Si_2$, $TbCo_2Ge_2$ and $DyCo_2Ge_2$, J. Alloys Compd. **190**, L23 (1992).

[24] D. Gignoux and D. Schmitt, Metamagnetism and complex magnetic phase diagrams of rare earth intermetallics, J. Alloys Compd. **225**, 423 (1995); Proceedings of the 2nd International Conference on f-Elements.

[25] M. A. Khan, Q. Zhang, J.-K. Bao, R. S. Fishman, A. S. Botana, Y. Choi, G. Fabbris, D. Haskel, J. Singleton, and J. F. Mitchell, Steplike metamagnetic transitions in a honeycomb lattice antiferromagnet $Tb_2Ir_3Ga_9$, Phys. Rev. Mater. **3**, 114411 (2019).

[26] S. H. Curnoe, Effective spin-1/2 exchange model for $Tb_2Ti_2O_7$, Phys. Rev. B **88**, 014429 (2013).

[27] S. M. Winter, Y. Li, H. O. Jeschke, and R. Valentí, Challenges in design of Kitaev materials: Magnetic interactions from competing energy scales, Phys. Rev. B **93**, 214431 (2016).

[28] Q. Luo, S. Hu, B. Xi, J. Zhao, and X. Wang, Ground-state phase diagram of an anisotropic spin-$\frac{1}{2}$ model on the triangular lattice, Phys. Rev. B **95**, 165110 (2017).

[29] P. A. Maksimov, Z. Zhu, S. R. White, and A. L. Chernyshev, Anisotropic-Exchange Magnets on a Triangular Lattice: Spin Waves, Accidental Degeneracies, and Dual Spin Liquids, Phys. Rev. X **9**, 021017 (2019).

[30] F. Ye, Z. Morgan, W. Tian, S. Chi, X. Wang, M. E. Manley, D. Parker, M. A. Khan, J. F. Mitchell, and R. Fishman, Canted antiferromagnetic order and spin dynamics in the honeycomb-lattice compound $Tb_2Ir_3Ga_9$, Phys. Rev. B **103**, 184413 (2021).

[31] For the model in Ref. [[30] online], the interactions between layers help produce the magnetization jumps. Consequently, the interaction J_1 between sites 1 and 2 or 3 and 4 on each layer are negligible.

[32] C. Liu, R. Yu, and X. Wang, Semiclassical ground-state phase diagram and multi-q phase of a spin-orbit-coupled model on triangular lattice, Phys. Rev. B **94**, 174424 (2016).

[33] S. Li, Magnetic field induced phase transitions of the triangular spin model, Phys. Rev. B **103**, 104421 (2021).

[34] J. Chaloupka and G. Khaliullin, Hidden symmetries of the extended Kitaev-Heisenberg model: Implications for the honeycomb-lattice iridates Na2IrO3, Phys. Rev. B **92**, 024413 (2015).

[35] P. A. Maksimov and A. L. Chernyshev, Rethinking $RuCl_3$, Phys. Rev. Res. **2**, 033011 (2020).

[36] F. Stegemann, Y. Zhang, B. P. T. Fokwa, and O. Janka, On the formation of the $Gd_3Ru_4Al_{12}$ versus the $Y_2Co_3Ga_9$ type structure - $M_3Rh_4Al_{12}$ (M = Ca, Eu) versus $M_2T_3Al_9$ (M = Ca, Sr, Eu, Yb; T = Ir, Pt), Dalton Trans. **49**, 6398 (2020).

[37] K. R. Meihaus, M. E. Feiser, J. F. Corbey, W. Evans, and J. R. Long, Record high single-ion magnetic moments through $4f^n5d^1$ electron configurations in the divalent lanthanide complexes $[(C_5H_4SiMe_3)_3Ln]^-$, J. Am. Chem. Soc. **137**, 9855 (2015).

[38] A. J. Ryan, L. E. Darago, S. G. Balasubramani, G. P. Chen, J. W. Ziller, F. Furche, J. R. Long, and W. J. Evans, Synthesis, structure, and magnetism of tris(amide) $[Ln\{N(SiMe_3)_2\}_3]^{1-}$ complexes of the non-traditional +2 lanthanide ions, Chem. Eur. J. **24**, 7702 (2018).

[39] C. A. Gould, K. R. McClain, J. M. Yu, T. J. Groshens, F. Furche, B. G. Harvey, and J. R. Long, Synthesis and magnetism of neutral, linear metallocende complexes of terbium(II) and dysprosium(III), J. Am. Chem. Soc. **141**, 12967 (2019).